Article:

He, T orcid.org/0000-0001-8975-8667, Wignall, PB orcid.org/0000-0003-0074-9129, Newton, RJ orcid.org/0000-0003-0144-6867 et al. (4 more authors) (2022) Extensive marine anoxia in the European epicontinental sea during the end-Triassic mass extinction. Global and Planetary Change, 210. 103771. p. 103771. ISSN 0921-8181

https://doi.org/10.1016/j.gloplacha.2022.103771

Extensive marine anoxia in the European epicontinental sea during the end-Triassic mass extinction

Tianchen He*, Paul B. Wignall, Robert J. Newton, Jed W. Atkinson, Jacob F. J. Keeling, Yijun Xiong, Simon W. Poulton

School of Earth and Environment, University of Leeds, Leeds LS2 9JT, UK.

* Corresponding author. *E-mail address:* T.He@leeds.ac.uk (T. He).

ABSTRACT

Warming-induced marine anoxia has been hypothesized as an environmental stressor for the end-Triassic mass extinction (ETME), but links between the spread of marine anoxia and the two phases of extinction are poorly constrained. Here, we report iron speciation and trace metal data from the Bristol Channel Basin and Larne Basin of the NW European epicontinental sea (EES), spanning the Triassic–Jurassic (T–J) transition (~ 202-200 Ma). Results show frequent development of anoxic-ferruginous conditions, interspersed with ephemeral euxinic episodes in the Bristol Channel Basin during the latest Rhaetian, whereas the contemporaneous Larne Basin remained largely oxygenated, **suggesting heterogeneous redox conditions between basins.** Subsequently, more persistent euxinic conditions prevailed across the T–J boundary in both basins, coinciding precisely with the second phase of the ETME. **We propose that this later phase of benthic faunal loss in the NW EES was directly driven by the bottom-water oxygen crisis.** Conversely, although anoxic conditions persisted into the early Hettangian, the benthos diversified at this time **in nearshore areas**. **Post-extinction conditions were poised at a fluctuating redox state, but anoxia did not extend into the shallowest areas where benthic marine ecosystem recovery was occurring**.

Keywords: Marine anoxia; European epicontinental sea; Iron speciation; Trace metals; End-Triassic extinction

1. Introduction

The end-Triassic mass extinction (ETME) was one of the five largest biotic turnovers in the geologic record (Wignall, 2015). The crisis was closely linked to eruptions of the Central Atlantic magmatic province (CAMP), and the associated massive greenhouse gas emissions are thought to have triggered rapid warming (McElwain et al., 1999; Pálfy and Smith, 2000; Ruhl et al., 2011). Nevertheless, the direct trigger for marine ecosystem collapse is debated, with causes such as ocean acidification and anoxia being amongst the favoured mechanisms (Ward et al., 2004; Greene et al., 2012; Fox et al., 2020, 2021). Isotope records from seawater sulfate and uranium have shown clear evidence for short-lived, but pervasive development of marine anoxia on a global scale, coinciding precisely with the extinction interval (Jost et al., 2017; He et al., 2020). Regional marine sediment nitrogen and sulfur isotope records (Luo et al., 2018; Fujisaki et al., 2020) and biomarkers (Richoz et al., 2012; Beith et al., 2021; Fox et al., 2021) demonstrate the development of brief anoxia on the deeper parts of the shelves and slopes in the latest Rhaetian, with subsequent expansion of euxinia into shallow settings in the early Hettangian. Conversely, conditions on the Panthalassa ocean floor remained fully oxygenated across the ETME (Hori et al., 2007; Wignall et al., 2010; Fujisaki et al., 2020).

Existing evidence for shelf anoxia provides only indirect measurements of redox conditions, but more direct proxies (*e.g.*, iron speciation linked to redox sensitive trace metal systematics) are available to assess local water-column redox conditions. Furthermore, Wignall and Atkinson (2020) have recently shown that the ETME was divided into two separate extinction phases, occurring in the late Rhaetian and immediately below the Triassic–Jurassic (T–J) boundary. However, the precise nature of the correlation between marine redox conditions in the EES and the two crisis events is not well constrained.

Here we report the first combined Fe speciation and trace metal analyses from three marine siliciclastic successions of the NW EES, which provide a continuous record of water column redox evolution through the latest Rhaetian to early Hettangian. These successions include the **relatively offshore** St Audrie's Bay (STAB) and Lilstock (LILS) sections from the Bristol Channel Basin of southwestern England, and **the more proximal** Larne section from the Larne Basin (LB) of Northern Ireland. Our data show evidence for an extensive spread of marine anoxia throughout the T–J transition, and the development of highly inhospitable euxinic conditions associated with the second phase of the ETME.

2. Palaeogeography and stratigraphic settings

The stratigraphic units straddling the T–J boundary at the STAB, LILS and LN sections were deposited in the western part of the EES (Fig. 1) and represent a regressive-transgressive cycle (Wignall and Atkinson, 2020). Regression is manifest in a shallowing-up succession from the marine mudstone/shale facies in the Westbury Formation, into shallower siltstone-rich lithofacies of the lower-mid Cotham Member of the Lilstock Formation, where a widespread desiccation horizon is developed (Wignall and Bond, 2008) (Fig. 2). The upper Cotham Member marks the onset of transgression (Hallam and Wignall, 1999), beginning with brackish facies which typically comprise limestones and calcareous marl-mudstones in the **shallower** Larne Basin (Simms, 2007; Simms and Jeram, 2007; Morton et al., 2017), and thinly-bedded marls and fine-grained sandstone in the Bristol Channel Basin. With continued sea-level rise, a fully marine fauna developed in the overlying Langport Member, which comprises micritic limestones and calcareous muds in the Bristol Channel area (Swift, 1999), and interbedded siltstones and mudstones at the Larne section (Simms and Jeram, 2007). The Blue Lias (SW England) and Waterloo Mudstone (Larne section) formations represent the lowest units of the Jurassic, and comprise interbedded organic-rich shales, marls and limestones (Wignall, 2001; Hesselbo et al., 2002; Atkinson and Wignall, 2019; Wignall and Atkinson, 2020). The lowest part of both formations consists of the Pre-*planorbis* Beds (Hesselbo et al., 2002) (Fig. 2). At the STAB section, the studied succession continues up to the *Liasicus* Zone of the mid-Hettangian, which mainly comprises black shale and mudstone.

The stratigraphic correlation between the Bristol Channel and Larne areas (Fig. 2) is based upon biostratigraphic and lithostratigraphic correlation (Simms and Jeram, 2007; Atkinson and Wignall, 2019, 2020) and further corroborated by a new carbon isotope record at the Larne section (Jeram et al., 2021). The Rhaetian Westbury and Lilstock formations contain an abundant but fairly low diversity euryhaline fauna dominated by bivalves and ostracods, and lesser numbers of gastropods, corals, conodonts and echinoderms (Wignall and Atkinson, 2020). The overlying Hettangian Blue Lias and Waterloo Mudstone formations are characterized by an abundant and diversifying fauna dominated by bivalves, including *Plagiostoma*, *Gryphaea* and *Pinna*, and ammonites (Atkinson and Wignall, 2019, 2020; Wignall and Atkinson, 2020). Detailed investigation of the ranges of bivalves, ostracods and conodonts in the British Isles and across the western EES, have revealed two distinct extinction horizons, the first in the lower part of the Cotham Member and the second at the top of the Langport Member (Fig. 2). These horizons were immediately followed by trends of increasing benthic macrofaunal diversity (Wignall and Atkinson, 2020).

3. Material and methods

3.1. Samples

A total of 100 mudstone, black shale and marl samples were collected from the STAB (ST 103 432) and LILS (ST 179 453) sections in southwestern England, and the LB section (Irish Grid Ref D409 037) in Northern Ireland. Associated sandstone lithofacies were not analyzed. Weathered surfaces or crusts of the whole-rock samples were first removed using a diamond-tipped saw. The cleaned rock slabs were then crushed and ground to fine powder using an agate disc mill.

3.2. Fe speciation

Fe speciation is widely used to distinguish water-column redox conditions, ranging from fully oxic, through anoxic-ferruginous, to anoxic-euxinic states (Poulton and Canfield, 2011; Poulton, 2021). These states are determined by evaluating the abundance of the highly reactive iron (Fe_{HR}) fraction relative to the total iron pool. Fe_{HR} phases include carbonate associated iron (Fe_{carb}), pyrite (Fe_{PY}), ferric oxides (Fe_{ox}) and magnetite (Fe_{mag}). Sequential extraction of Fe_{HR} phases was performed according to the standard chemical protocol described by Poulton and Canfield (2005). Around 100 mg of sample powder was first treated with a sodium acetate solution at pH 4.5 and 50 °C for 48 h to extract Fe_{carb}. Fe_{ox} was then extracted via a sodium dithionite solution at pH 4.8 and room temperature for 2 h. This was followed by the final leaching of Fe_{mag} with an ammonium oxalate solution at room temperature for 6 h. The concentration of these iron phases was measured using a ThermoFisher iCE 3300 atomic absorption spectrometer (AAS) in the Cohen Geochemistry Laboratory, University of Leeds. Pyrite Fe (Fe_{PY}) was extracted following the chromous chloride distillation method (Canfield et al., 1986). The concentration of Fe_{PY} was calculated stoichiometrically by the weight of precipitated silver sulfide from the extraction. Replicate extractions of samples and reference material WHIT (Alcott et al., 2020) yielded relative standard deviations (RSDs) of < 5 % for all highly reactive Fe phases.

3.3. Total digestion and bulk elemental concentrations

Approximately 100 mg of sample powder was first ashed for 8 h at 550 °C to remove organic matter. Total digestion of the residue was performed using an acid combination of HNO_3-HF-$HClO_4$. Boric acid was used to prevent the formation of Al complexes. An aliquot of the resulting solution was measured for concentrations of Al using a ThermoFisher iCAP 7400 radial inductively coupled plasma optical emission spectrometer (ICP-OES), and trace metals (Mo and U) using a ThermoFisher iCAP Qc inductively coupled plasma mass spectrometer (ICP-MS) in the Cohen Geochemistry Laboratory, University of Leeds. Total Fe concentrations (Fe_T) were measured using a ThermoFisher iCE 3300 atomic absorption spectrometer (AAS).

Accuracy was monitored by analyzing certified reference materials USGS Eocene Green River Shale (SGR-1). Repeated measurement of samples yielded RSDs for all elements of better than 3%.

4. Results and discussions

4.1. Water column redox proxies

Here we combine proxy evidence from sediment Fe speciation and trace metal abundances to constrain water column redox variability through the T–J transition in the Bristol Channel Basin and Larne Basin (see data in Table S1). Calibrations in modern and ancient marine environments suggest that sediments are enriched in highly reactive iron (Fe_{HR}) in an anoxic water column ($Fe_{HR}/Fe_T > 0.38$) in contrast to fully oxic conditions, where Fe_{HR}/Fe_T ratios are commonly < 0.22 (Poulton and Canfield, 2011). The enrichment of redox-sensitive U can provide independent constraints on anoxic conditions (Algeo and Tribovillard, 2009; Tribovillard et al., 2012). Under reducing conditions, U(VI) in seawater is reduced to less soluble U(IV), promoting authigenic enrichment of U in the sediments relative to the average crustal abundance (e.g., upper continental crust (UCC)) (Rudnick and Gao, 2014). The reduction of U starts at the Fe (II)–Fe (III) redox boundary and links directly with Fe redox reactions rather than the presence of free H_2S in the water column (i.e., euxinia).

The precise nature of anoxic depositional conditions can be further evaluated by examining the relative proportion of pyrite in the Fe_{HR} pool, where a ferruginous (anoxic, Fe^{2+} rich and sulfide-free) water column generally yields Fe_{PY}/Fe_{HR} lower than 0.6-0.8, with euxinic conditions diagnosed above this threshold (Poulton, 2021). The redox evaluation can be supported by investigation of Mo systematics. Mo is present as the molybdate anion in the modern oxic ocean, but in euxinic settings, seawater Mo is converted to particle-reactive thiomolybdate or is associated with authigenic iron sulfides, leading to excess Mo enrichments and elevated Mo/U ratios relative to oxic and ferruginous settings (Algeo and Lyons, 2006).

4.2. Marine redox variations in the late Rhaetian

Enrichments in highly reactive Fe ($Fe_{HR}/Fe_T > 0.38$) in siliciclastic samples occur throughout the Westbury and Lilstock formations in the STAB and LILS sections (Fig. 3a & 4a), suggesting that anoxic water column conditions were a prevalent feature of late Rhaetian deposition in the Bristol Channel Basin. These elevated Fe_{HR}/Fe_T ratios coincide with U/Al ratios that are higher than the average composition of UCC (Rudnick and Gao, 2014) (Fig. 3d & 4d). Furthermore, samples that are increasingly enriched in Fe_{HR}/Fe_T (above the oxic-anoxic boundary of 0.38) also show a progressive enrichment in U/Al (Fig. 6a), clearly supporting anoxic intervals, with co-enrichment in Fe_{HR} and U as the overall intensity or persistence of anoxia increased. However, benthic macrofossils are abundant and diverse throughout most of these Rhaetian sediments (Wignall and Atkinson, 2020), which indicates that the anoxic conditions were not persistent; oxygenated conditions and benthic colonization was likely frequent but short lived. Thus, water column redox conditions during this commonly anoxic interval in the late Rhaetian, as recorded by geochemical proxy evidence, may have fluctuated between anoxic and oxic conditions on a variety of timescales.

The majority of late Rhaetian samples in the Bristol Channel Basin show Fe_{PY}/Fe_{HR} values scattering around the equivocal zone (0.6-0.8) (Fig. 3b and 4b), which may represent either anoxic-ferruginous or euxinic condition (Poulton, 2021). However, only a few of these samples exhibit co-enrichments in Mo/Al and Mo/U (Figs. 3e,f and 4e,f), suggesting that euxinic conditions **were rare**. Therefore, when anoxic deposition occurred in the Westbury Formation to upper Langport Member of the Bristol Channel Basin, it was dominated by ferruginous conditions interspersed with ephemeral euxinic episodes (Fig. 3g, 4g and 7a). In detail, it is noteworthy that the upper part of the Cotham Member shows **a mixture of ferruginous and euxinic conditions** at a level considered to be brackish, based on the presence of ostracods and conchostracans (Morton et al., 2017), implying deposition in a restricted, possibly lagoonal, setting. The redox conditions in the lower part of the Cotham Member were not assessed because of the unsuitable siltstone and sandstone lithologies at this level, and thus the oxygenation regime at the time of the first phase of extinction remains unresolved. The shale horizons of the Langport Formation at the STAB and LILS sections generally record anoxic-ferruginous conditions (Figs. 3g and 4g). In sharp contrast to the Bristol Channel Basin, sediments in the **shallower** Larne Basin have Fe_{HR}/Fe_T ratios lower than 0.38 across most of the late Rhaetian, suggesting that fully oxic conditions were dominant (Fig. 5a,g).

Nonetheless, samples from both the upper Cotham and Langport members show rising trends of elevated Fe_{HR}/Fe_T ratios (> 0.38) and higher Fe_{HR}/Fe_T ratios coincide with relatively higher U/Al values (Fig. 5a,d), which are suggestive of intervals of **more persistent** anoxic-ferruginous conditions (Fig. 5g). **Dominantly** euxinic conditions only developed around the base of the Waterloo Mudstone Formation, in the Pre-*planorbis* Beds. **This intensification of anoxia, to the point of persistent euxinia**, is seen in all our study sites, and coincides with the second phase of the ETME. Independent evidence from aryl isoprenoids and isorenieratane occurrences (Beith et al., 2021), also support the presence of photic zone euxinia in the Bristol Channel Basin during this interval.

4.3. Enhanced redox fluctuations through the early Hettangian

Euxinic conditions persisted during deposition of the Pre-*planorbis* Beds in the Bristol Channel Basin, as demonstrated by elevated ratios of Fe_{PY}/Fe_{HR} (> 0.7), Mo/Al and Mo/U (Figs. 3 and 4). This is immediately followed by a transition towards a more fluctuating redox state in the Hettangian *planorbis* and *liasicus* zones that alternates between anoxic-ferruginous and euxinic (Figs. 3g and 7c). By contrast, in the Larne Basin, while lower Hettangian samples are dominated by Fe_{HR}/Fe_T ratios higher than 0.38, Fe_{PY}/Fe_{HR} ratios are commonly below 0.6 (Fig. 5a,b). The U/Al record fluctuates during this interval in the Larne Basin (Fig. 5d), but some values are elevated relative to UCC, supporting frequent development of anoxic-ferruginous conditions in the water column (Fig. 7c). However, the post-extinction lower Hettangian sediments in these basins **contain a benthic fauna dominated by bivalves** that indicate transient oxygenation (Atkinson and Wignall, 2019, 2020).

4.4. Marine redox landscape and ecosystem changes in the EES through the T–J transition

Our new redox analyses reveal that anoxic-ferruginous waters were common in the late Rhaetian, and this was followed by the sporadic spread of euxinia in the Bristol Channel Basin. However, the facies associated with the first ETME phase in the lower Cotham Member record very shallow-water conditions and are not suitable for redox analysis. In the Bristol Channel Basin, the first extinction phase occurs just below a widespread emergence surface with large desiccation cracks (Wignall and Bond, 2008). The contemporaneous Larne Basin section was also developed **in a basin margin location** and remained well-oxygenated during deposition of the Cotham Member (Fig. 7). The role of anoxia in the first extinction phase is therefore unclear and requires study of more offshore sections than are available in the British Isles.

By contrast, the intensification of euxinia across the two basins during the second phase of the ETME is clear (Fig. 7b). Thus, the spread of euxinic waters likely caused contraction of ecological habitable zones, and resulted in the dwarfing and high extinction rates observed at this time (Wignall and Atkinson, 2020). Commonly euxinic waters continued to develop in the Bristol Channel Bains and Larne Basin through the early Hettangian (Fig. 7c). The low oxygen conditions did not hinder long-term ecosystem recovery in the Early Jurassic because nearshore areas, seen for example in South Wales, deposited under fully oxygenated conditions and thus acted as the cradle of recovery in the region (Atkinson and Wignall, 2019, 2020). The euxinic intervals in basinal settings of the early Hettangian alternated with oxic water column conditions, as evidenced by the sporadic presence of benthic macrofaunal and bioturbation in these sediments.

Our findings are supported by contemporaneous isotopic evidence for the behavior of seawater sulfate in the wider EES. A positive S-isotope excursion in seawater sulfate was identified in the Cotham Member in the Larne Basin, indicating a short-lived marine deoxygenation pulse (He et al., 2020). Records of sedimentary pyrite S-isotopes also demonstrate that the upper Rhaetian of the Bristol Channel Basin (Jaraula et al., 2013) and other basins of the eastern EES (Luo et al., 2018) were characterised by brief anoxic/euxinic events during the extinction intervals. Additional data from green sulfur-derived biomarkers indicate recurring photic zone euxinia through the T–J transition in both the Bristol Channel Basin and the Cleveland Basin of North Yorkshire (Jaraula et al., 2013; Beith et al., 2021; Fox et al., 2021). **On a global scale, contemporaneous anoxia-hypoxia was widespread across the ETME in the shallow and mid-depth waters of the western Tethys and eastern Panthalassa (Jost et al., 2017; He et al., 2020, 2022).**

The reasons for the extensive or sporadic occurrence of anoxia in the EES and wider ocean during the ETME could plausibly be related to extreme hyperthermal conditions (Ruhl et al., 2011). The ETME was closely linked to the contemporaneous emplacement of the CAMP through the Late Triassic–Early Jurassic transition (Ruhl et al., 2010, 2011; Blackburn et al., 2013; Thibodeau et al., 2016; Davies et al., 2017; Korte et al., 2018; Marzoli et al., 2018). Global warming may therefore have driven ocean deoxygenation and stratification (Jaraula et al., 2013; Luo et al., 2018; Fujisaki et al., 2020). Furthermore, low seawater sulfate concentrations across the T–J transition would have promoted benthic methane release, thereby exacerbating the intensity of bottom-water anoxia (He et al., 2020).

5. Conclusions

Sediment Fe speciation and trace metal data from two representative basins of the NW EES, provide a near-complete record of water column redox conditions through the T–J transition. Our data suggest an oscillating redox state that commonly saw anoxic-ferruginous or euxinic conditions develop in the Bristol Channel Basin and Larne Basin. We also identify spatial redox variability in the latest Triassic between the Bristol Channel Basin and the Larne Basin, with the latter developing more oxygenated conditions through this interval, likely due to shallower water depths. Although no definite anoxia-extinction link is seen during the first phase of the ETME in the latest Rhaetian, when sea-level fell and an emergent horizon developed, a shift towards intensified euxinia occurred in the latest Rhaetian. **This marks a major environmental deterioration event associated with the second ETME phase.** We thus propose that oxygen deficiency was a direct driver for the second phase of the ETME in the NW EES. Further studies in deeper water settings are required to constrain redox conditions during the first ETME phase.

During the post-extinction early Hettangian, anoxic-ferruginous or euxinic conditions persisted in the EES basins, but the region was characterised by highly dynamic, fluctuating redox conditions on various timescales.

Declaration of competing interest

The authors declare that they have no known competing financial interests or personal relationships that could have appeared to influence the work reported in this paper.

Acknowledgements

This work was supported by the Natural Environment Research Council (grant NE/N018559/1) and the National Natural Science Foundation of China (41888101, 41902026). We also acknowledge funding from the International Continental Scientific Drilling Program. This manuscript is a contribution to the Integrated Understanding of the Early Jurassic Earth System and Timescale (JET) project and IGCP 739. We thank M. Simms for fieldwork assistance in the Larne Basin. We thank R. Corns of Natural England for granting sampling permission in Somerset. We thank S. Reid, A. Hobson and A. Connelly for assistance in the labs. We also thank I. Boomer, R.L. Silva amd H. Wu for valuable discussions.

Appendix. Table S1

Supplementary data to this article can be found at Table S1.

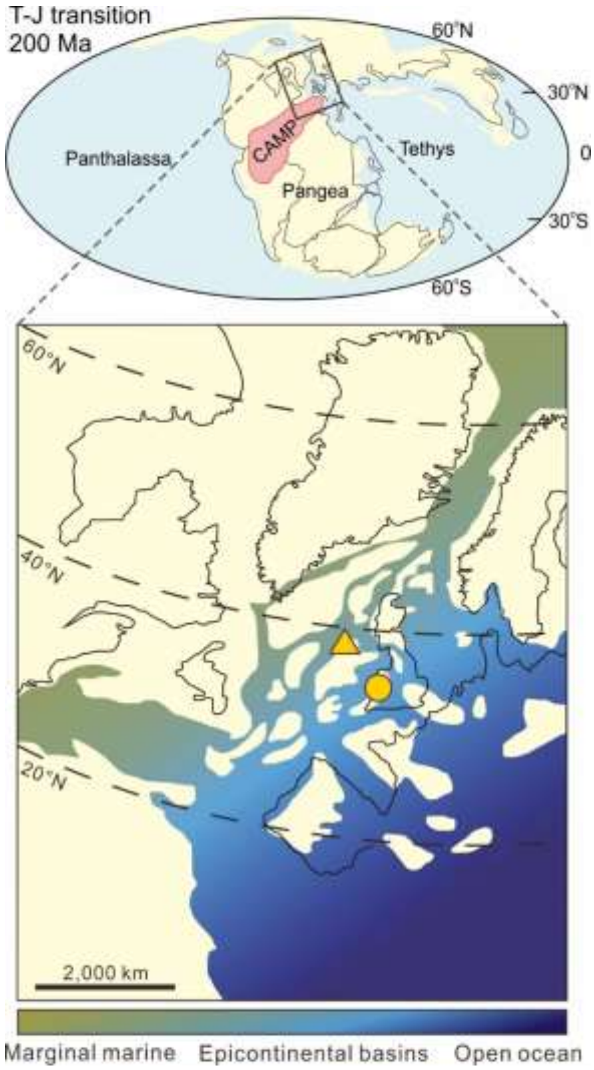

Fig. 1. Paleogeographical map for the Triassic–Jurassic (T–J) transition showing localities for studied sections of NW European epicontinental sea. This figure is reprinted from the work of Richoz et al. (2012) and He et al. (2020). Yellow filled circle indicates the location of St. Audrie's Bay section and Lilstock section in the Bristol Channel Basin, southwestern England. Yellow filled triangle indicates the location of Larne section in the Larne Basin, Northern Ireland. CAMP: Central Atlantic Magmatic Province.

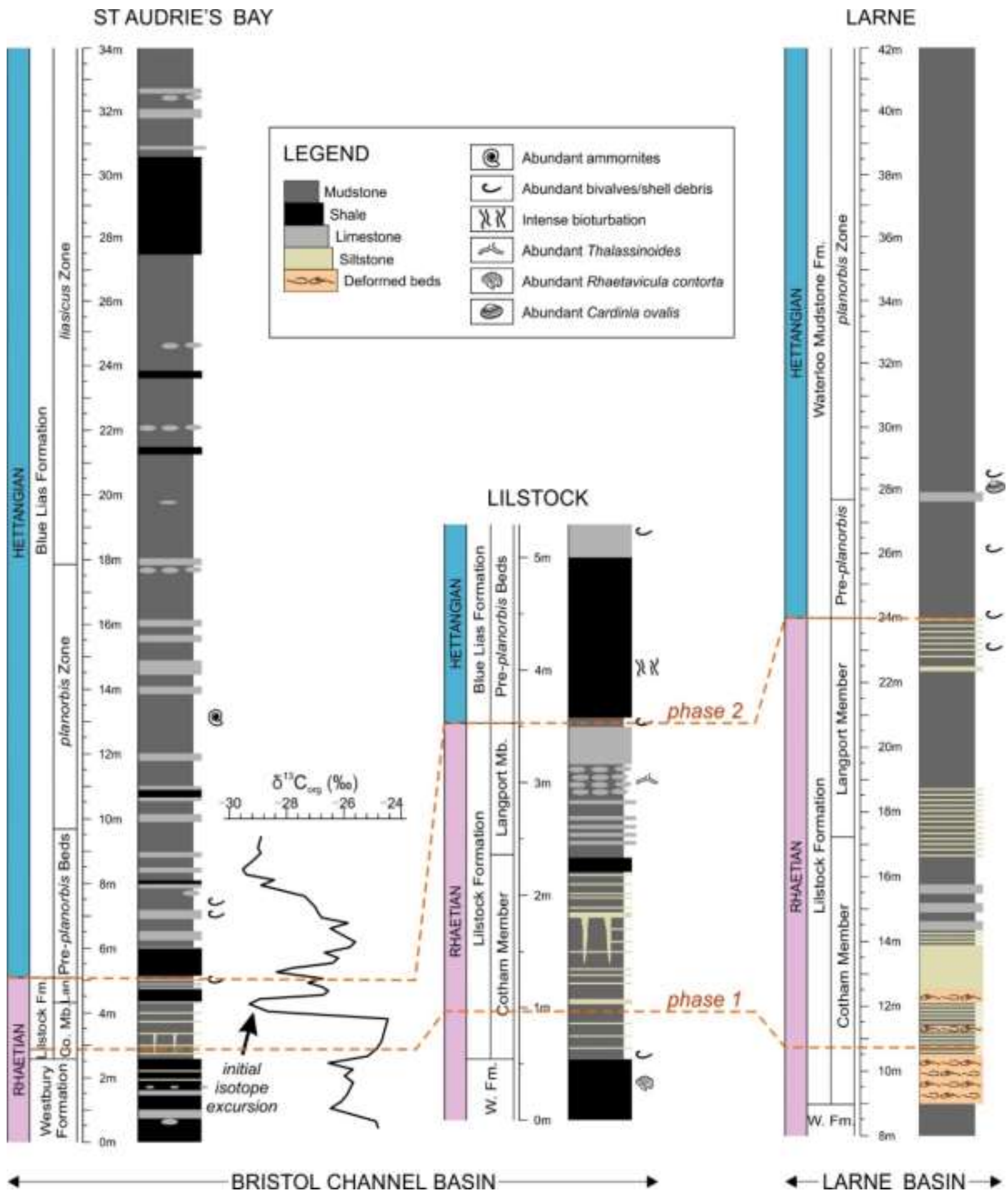

Fig. 2. Rhaetian–Hettangian stratigraphy of the St Audrie's Bay, Lilstock and Larne sections. Stratigraphic depth and the lithological log are presented alongside the global stages and regional biozones. **Stratigraphic correlation for lithological units and positions of extinction are based on biostratigraphic and lithostratigraphic data (Atkinson and Wignall, 2019, 2020).** W., Westbury Formation; Co., Cotham Member; Lan., Langport Member. Fm., Formation; Mb., Member. Organic carbon isotope ($\delta^{13}C_{org}$) data of St Audrie's Bay section are presented from the work of Hesselbo et al. (2002). Horizontal orange dash lines indicate the two-phase extinction events at the lower part of Cotham Member (phase 1) and the top of Langport Member (phase 2), respectively (Wignall and Atkinson, 2020).

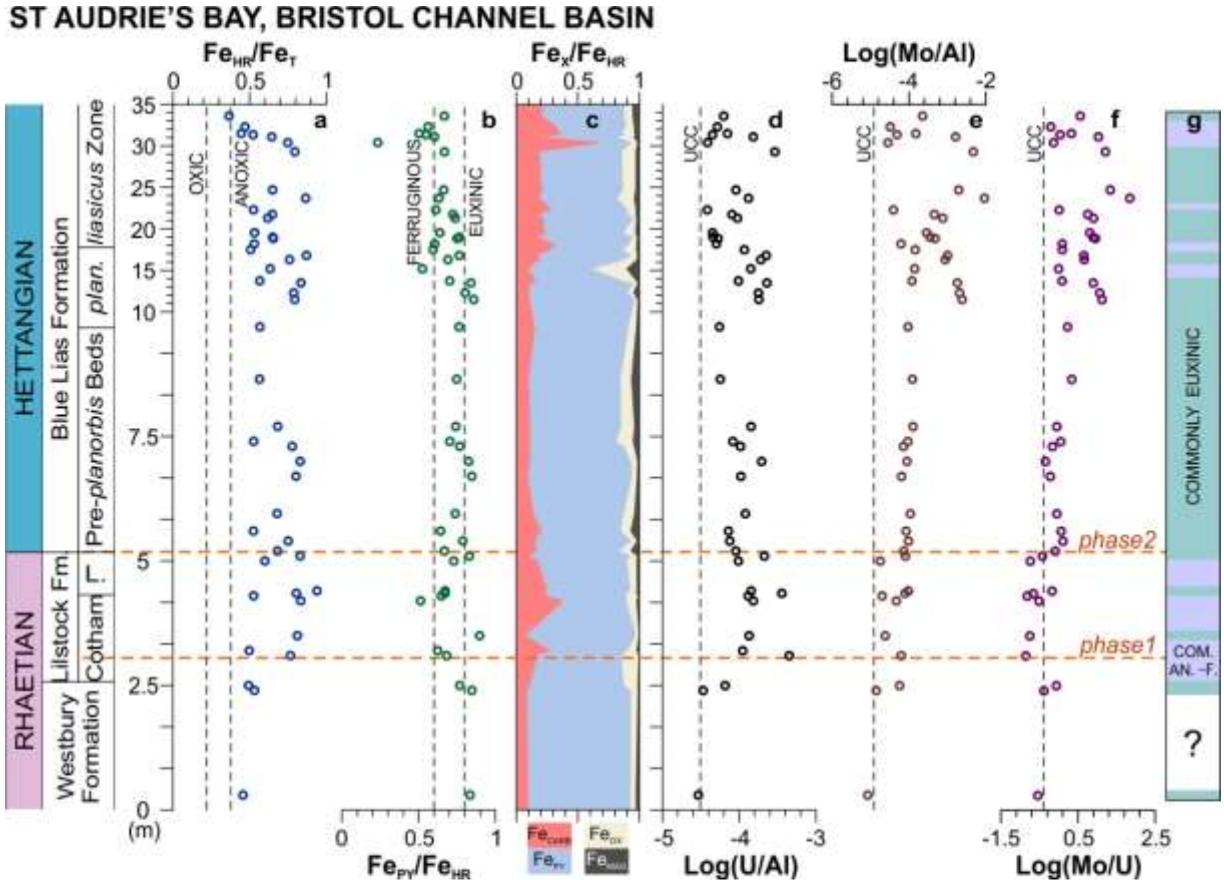

Fig. 3. Geochemistry of Fe speciation and trace metal from the St Audrie's Bay section, Bristol Channel Basin. a&b Iron speciation data: highly reactive iron to total iron ratios (Fe_{HR}/Fe_T); pyrite to highly reactive iron ratios (Fe_{PY}/Fe_{HR}); Vertical dash lines represent the thresholds for oxic ($Fe_{HR}/Fe_T < 0.22$) and anoxic ($Fe_{HR}/Fe_T > 0.38$), and ferruginous ($Fe_{PY}/Fe_{HR} < 0.6$) and euxinic ($Fe_{PY}/Fe_{HR} > 0.8$) depositional conditions. Fe_{HR}/Fe_T ratios between 0.22-0.38 and Fe_{PY}/Fe_{HR} ratios between 0.6-0.8 are considered equivocal and may represent either oxic or anoxic conditions, and ferruginous or euxinic conditions respectively (Poulton, 2021). **c** The proportion of different reactive iron phases within the total highly reactive Fe pool; Fe_{CARB}, carbonate-associated iron; Fe_{PY}, pyrite; Fe_{OX}, ferric oxides; Fe_{MAG}, magnetite. **d** U to Al ratios. **e** Mo to Al ratios. **f** Mo to U ratios. Elemental mass ratios are expressed as log([element]/[element]). Vertical dashed lines in d-f represent the mass ratios of average elemental compositions of upper continental crust (UCC) (Rudnick and Gao, 2014). **g** Variation in water column redox conditions: Commonly euxinic intervals (green bands); Commonly anoxic-ferruginous intervals (purple bands).

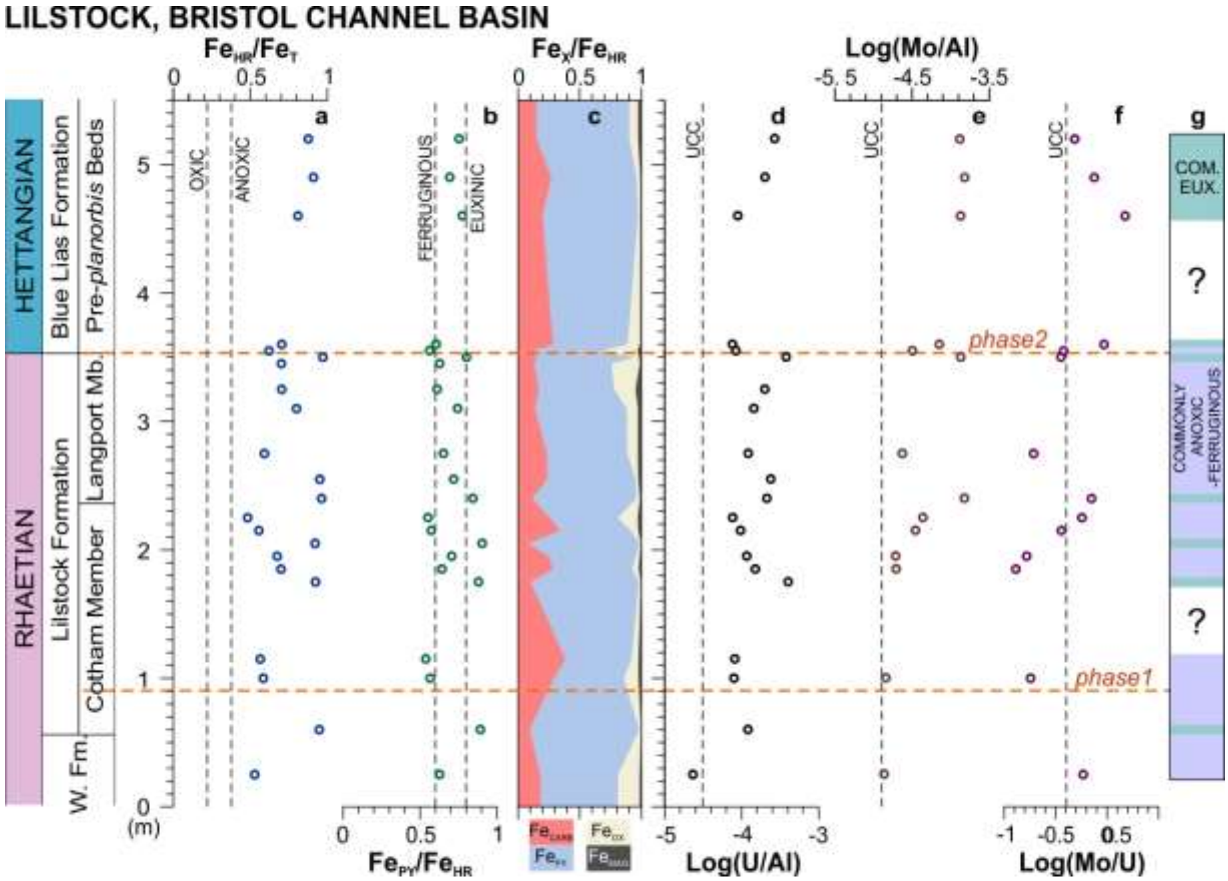

Fig. 4. Geochemistry of Fe speciation and trace metal from the Lilstock section, Bristol Channel Basin. a&b Iron speciation data. **c** The proportion of different reactive iron phases within the total highly reactive Fe pool. **d** U to Al ratios. **e** Mo to Al ratios. **f** Mo to U ratios. **g** Variation in water column redox conditions.

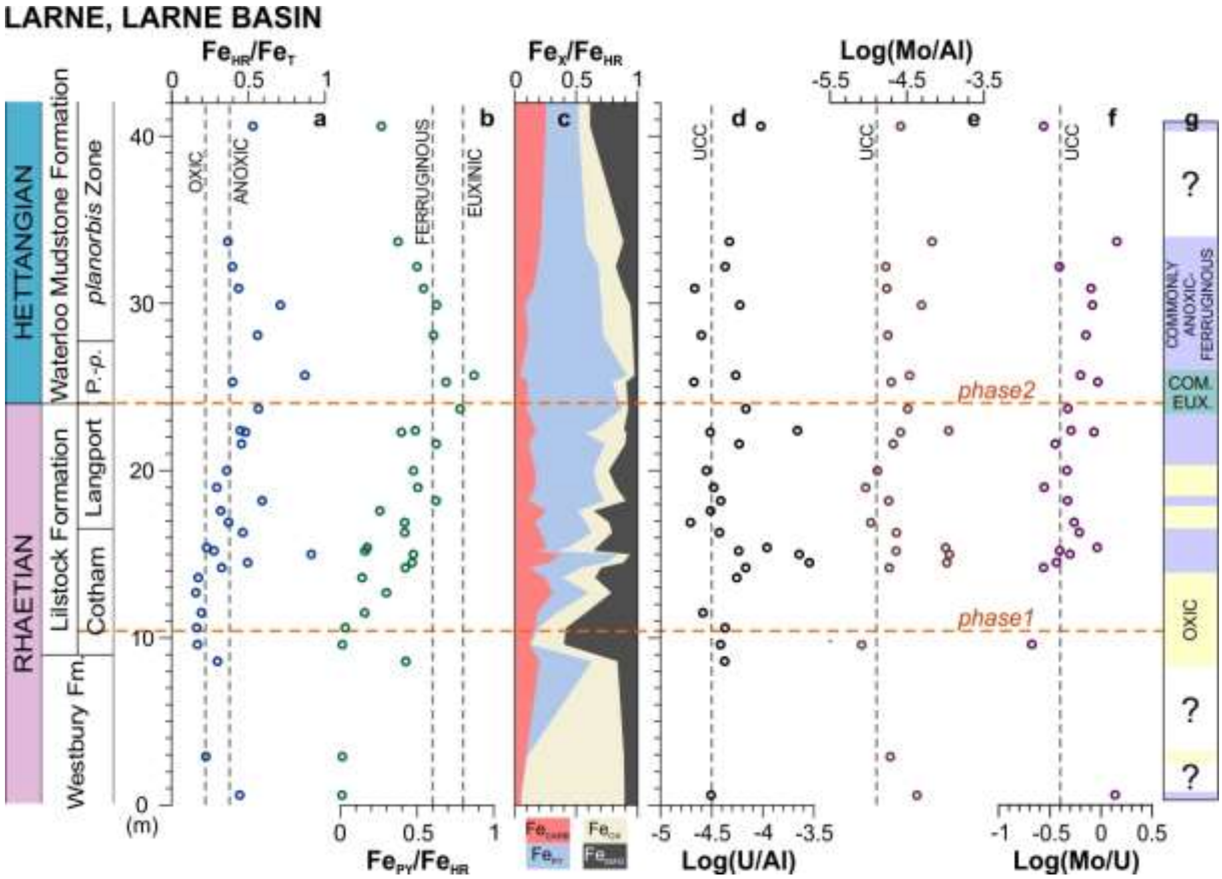

Fig. 5. Geochemistry of Fe speciation and trace metal from the Larne section, Larne Basin. **a&b** Iron speciation data. **c** The proportion of different reactive iron phases within the total highly reactive Fe pool. **d** U to Al ratios. **e** Mo to Al ratios. **f** Mo to U ratios. **g** Variation in water column redox conditions.

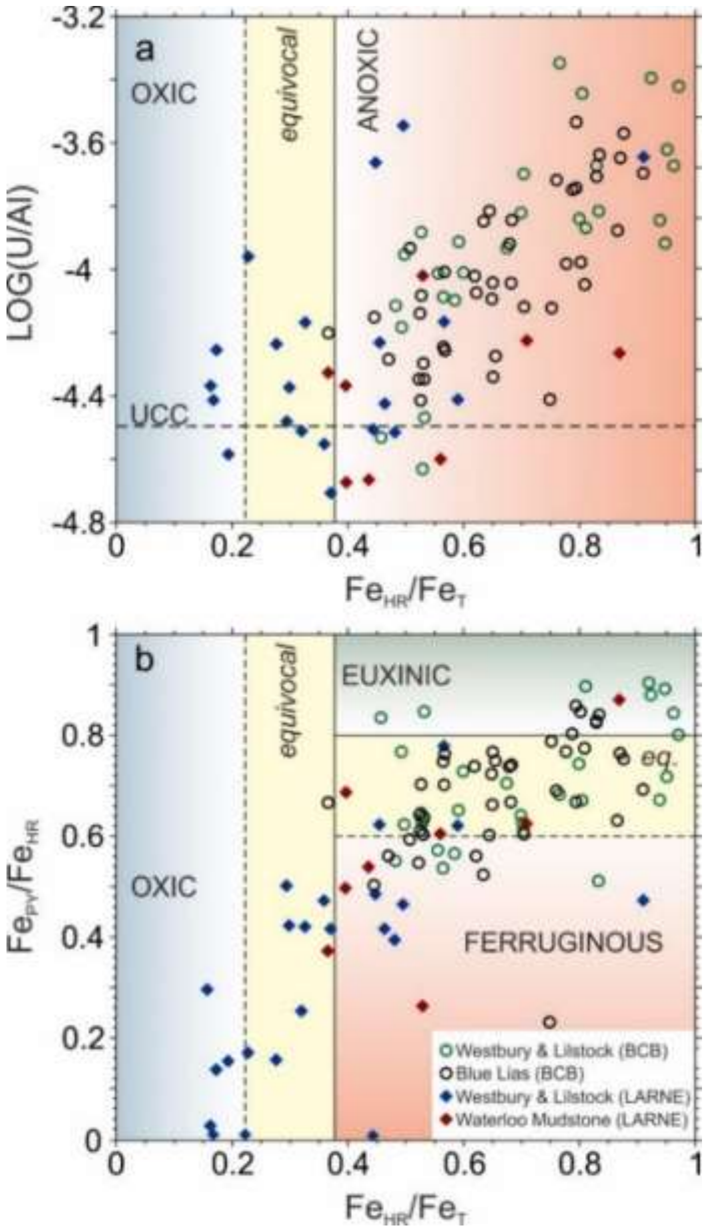

Fig. 6. Fe speciation and U concentration in Rhaetian–Hettangian sediments from the Bristol Channel Basin (BCB) and Larne Basin (LARNE). a U/Al versus Fe_{HR}/Fe_T. The horizontal dash line represents the average log(U/Al) value of UCC (Rudnick and Gao, 2014). **b** Figure shows the cross-plot of the ratios of pyrite Fe to highly reactive Fe (Fe_{PY}/Fe_{HR}) against highly reactive Fe to total Fe (Fe_{HR}/Fe_T). Thresholds are made for anoxic ($Fe_{HR}/Fe_T > 0.38$) and euxinic ($Fe_{PY}/Fe_{HR} > 0.8$) depositional conditions. Fe_{HR}/Fe_T ratios between 0.22-0.38 and Fe_{PY}/Fe_{HR} ratios between 0.6-0.8 are considered equivocal and may represent either oxic or anoxic conditions, and ferruginous or euxinic conditions respectively (Poulton, 2021).

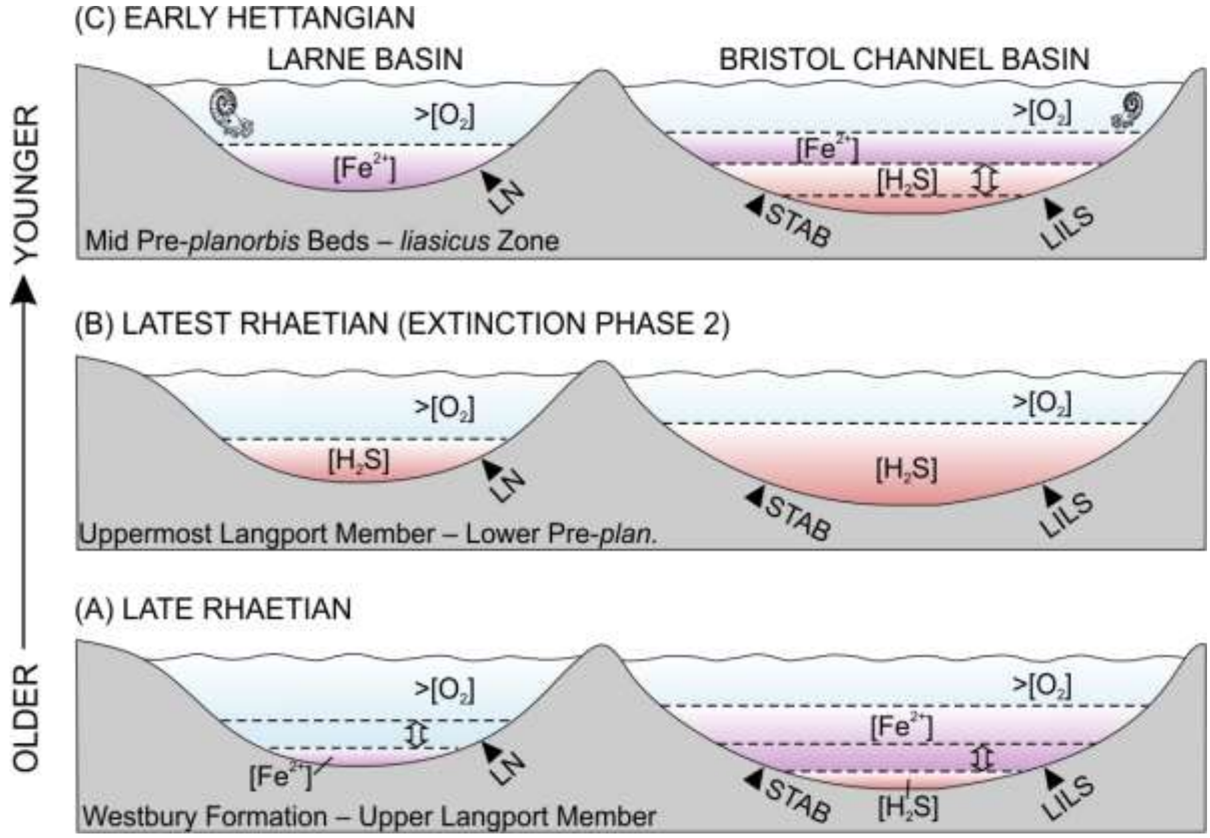

Fig. 7. Schematic diagram of water-column redox evolution in the Larne Basin and Bristol Channel Basin during the Rhaetian-Hettangian transition. LN, Larne section; STAB, St Audrie's Bay section; LILS: Lilstock section; Pre-*plan.*, Pre-*planorbis* Beds. Fully oxic conditions are indicated as >[O_2], whereas commonly anoxic-ferruginous or commonly euxinic conditions are demarcated with [Fe^{2+}] or [H_2S]. Dash lines in A-C represent chemocline or boundaries between oxic and anoxic zones. Arrows in A and C point out the directions of intermittent expansion/contraction of anoxic-ferruginous or euxinic zone. Note that neither of the suggested anoxic intervals were permanently developed, but represent a fluctuating state between persistent anoxia and more alternating oxic-anoxic.

References

Alcott, L.J., Krause, A.J., Hammarlund, E.U., Bjerrum, C.J., Scholz, F., Xiong, Y., Hobson, A.J., Neve, L., Mills, B.J.W., März, C., Schnetger, B., Bekker, A., Poulton, S.W., 2020. Development of Iron Speciation Reference Materials for Palaeoredox Analysis. Geostand. Geoanalytical Res. 44, 581–591. https://doi.org/10.1111/ggr.12342

Algeo, T.J., Lyons, T.W., 2006. Mo-total organic carbon covariation in modern anoxic marine environments: Implications for analysis of paleoredox and paleohydrographic conditions. Paleoceanography 21, 1–23. https://doi.org/10.1029/2004PA001112

Algeo, T.J., Tribovillard, N., 2009. Environmental analysis of paleoceanographic systems based on molybdenum–uranium covariation. Chem. Geol. 268, 211–225. https://doi.org/10.1016/j.chemgeo.2009.09.001

Atkinson, J.W., Wignall, P.B., 2020. Body size trends and recovery amongst bivalves following the end-Triassic mass extinction. Palaeogeogr. Palaeoclimatol. Palaeoecol. 538, 109453. https://doi.org/10.1016/j.palaeo.2019.109453

Atkinson, J.W., Wignall, P.B., 2019. How quick was marine recovery after the end-Triassic mass extinction and what role did anoxia play? Palaeogeogr. Palaeoclimatol. Palaeoecol. 528, 99–119. https://doi.org/10.1016/j.palaeo.2019.05.011

Beith, S.J., Fox, C.P., Marshall, J.E.A., Whiteside, J.H., 2021. Recurring photic zone euxinia in the northwest Tethys impinged end-Triassic extinction recovery. Palaeogeogr. Palaeoclimatol. Palaeoecol. 584, 110680. https://doi.org/10.1016/j.palaeo.2021.110680

Blackburn, T.J., Olsen, P.E., Bowring, S.A., McLean, N.M., Kent, D. V., Puffer, J., McHone, G., Rasbury, E.T., Et-Touhami, M., 2013. Zircon U-Pb Geochronology Links the End-Triassic Extinction with the Central Atlantic Magmatic Province. Science. 340, 941–945. https://doi.org/10.1126/science.1234204

Canfield, D.E., Raiswell, R., Westrich, J.T., Reaves, C.M., Berner, R.A., 1986. The use of chromium reduction in the analysis of reduced inorganic sulfur in sediments and shales. Chem. Geol. 54, 149–155. https://doi.org/10.1016/0009-2541(86)90078-1

Davies, J.H.F.L., Marzoli, A., Bertrand, H., Youbi, N., Ernesto, M., Schaltegger, U., 2017. End-Triassic mass extinction started by intrusive CAMP activity. Nat. Commun. 8, 15596. https://doi.org/10.1038/ncomms15596

Fox, C.P., Cui, X., Whiteside, J.H., Olsen, P.E., Summons, R.E., Grice, K., 2020. Molecular and isotopic evidence reveals the end-Triassic carbon isotope excursion is not from massive exogenous light carbon. Proc. Natl. Acad. Sci. U. S. A. 117, 30171–30178. https://doi.org/10.1073/pnas.1917661117

Fox, C.P., Whiteside, J.H., Olsen, P.E., Cui, X., Summons, R.E., Idiz, E., Grice, K., 2022. Two-pronged kill mechanism at the end-Triassic mass extinction. Geology.

https://doi.org/10.1130/G49560.1

Fujisaki, W., Fukami, Y., Matsui, Y., Sato, T., Sawaki, Y., Suzuki, K., 2020. Redox conditions and nitrogen cycling during the Triassic-Jurassic transition: A new perspective from the mid-Panthalassa. Earth-Science Rev. 204, 103173. https://doi.org/10.1016/j.earscirev.2020.103173

Greene, S.E., Martindale, R.C., Ritterbush, K.A., Bottjer, D.J., Corsetti, F.A., Berelson, W.M., 2012. Recognising ocean acidification in deep time: An evaluation of the evidence for acidification across the Triassic-Jurassic boundary. Earth-Science Rev. 113, 72–93. https://doi.org/10.1016/j.earscirev.2012.03.009

He, T., Dal Corso, J., Newton, R.J., Wignall, P.B., Mills, B.J.W., Todaro, S., Di Stefano, P., Turner, E.C., Jamieson, R.A., Randazzo, V., Rigo, M., Jones, R.E., Dunhill, A.M., 2020. An enormous sulfur isotope excursion indicates marine anoxia during the end-Triassic mass extinction. Sci. Adv. 6, eabb6704. https://doi.org/10.1126/sciadv.abb6704

He, T., Newton, R.J., Wignall, P.B., Reid, S., Dal Corso, J., Takahashi, S., Wu, H., Todaro, S., Di Stefano, P., Randazzo, V., Rigo, M., Dunhill, A.M., 2022. Shallow ocean oxygen decline during the end-Triassic mass extinction. Glob. Planet. Change (in press).

Hesselbo, S.P., Robinson, S.A., Surlyk, F., Piasecki, S., 2002. Terrestrial and marine extinction at the Triassic-Jurassic boundary synchronized with major carbon-cycle perturbation: A link to initiation of massive volcanism? Geology 30, 251. https://doi.org/10.1130/0091-7613(2002)030<0251:TAMEAT>2.0.CO;2

Hori, R.S., Fujiki, T., Inoue, E., Kimura, J.-I., 2007. Platinum group element anomalies and bioevents in the Triassic–Jurassic deep-sea sediments of Panthalassa. Palaeogeogr. Palaeoclimatol. Palaeoecol. 244, 391–406. https://doi.org/10.1016/j.palaeo.2006.06.038

Jaraula, C.M.B., Grice, K., Twitchett, R.J., Böttcher, M.E., LeMetayer, P., Dastidar, A.G., Opazo, L.F., 2013. Elevated $p\mathrm{CO_2}$ leading to Late Triassic extinction, persistent photic zone euxinia, and rising sea levels. Geology 41, 955–958. https://doi.org/10.1130/G34183.1

Jeram, A.J., Simms, M.J., Hesselbo, S.P., Raine, R., 2021. Carbon isotopes, ammonites and earthquakes: Key Triassic-Jurassic boundary events in the coastal sections of south-east County Antrim, Northern Ireland, UK. Proc. Geol. Assoc. 132, 702–725. https://doi.org/10.1016/j.pgeola.2021.10.004

Jost, A.B., Bachan, A., van de Schootbrugge, B., Lau, K. V., Weaver, K.L., Maher, K., Payne, J.L., 2017. Uranium isotope evidence for an expansion of marine anoxia during the end-Triassic extinction. Geochemistry, Geophys. Geosystems 18, 3093–3108. https://doi.org/10.1002/2017GC006941

Korte, C., Ruhl, M., Pálfy, J., Ullmann, C.V., Hesselbo, S.P., 2018. Chemostratigraphy Across the Triassic–Jurassic Boundary, in: Alcides N. Sial, Claudio Gaucher, Muthuvairavasamy Ramkumar, and V.P.F. (Ed.), Chemostratigraphy Across Major Chronological Boundaries. John Wiley & Sons, Inc., pp. 183–210. https://doi.org/10.1002/9781119382508.ch10

Luo, G., Richoz, S., van de Schootbrugge, B., Algeo, T.J., Xie, S., Ono, S., Summons, R.E., 2018. Multiple sulfur-isotopic evidence for a shallowly stratified ocean following the Triassic-Jurassic boundary mass extinction. Geochim. Cosmochim. Acta 231, 73–87. https://doi.org/10.1016/j.gca.2018.04.015

Marzoli, A., Callegaro, S., Dal Corso, J., Davies, J.H.F.L., Chiaradia, M., Youbi, N., Bertrand, H., Reisberg, L., Merle, R., Jourdan, F., 2018. The Central Atlantic Magmatic Province (CAMP): A Review, in: Tanner, L. (Ed.), The Late Triassic World. Springer, Cham, pp. 91–125. https://doi.org/10.1007/978-3-319-68009-5_4

McElwain, J.C., Beerling, D.J., Woodward, F.I., 1999. Fossil Plants and Global Warming at the Triassic-Jurassic Boundary. Science. 285, 1386–1390. https://doi.org/10.1126/science.285.5432.1386

Morton, J.D., Whiteside, D.I., Hethke, M., Benton, M.J., 2017. Biostratigraphy and geometric morphometrics of conchostracans (Crustacea, Branchiopoda) from the Late Triassic fissure deposits of Cromhall Quarry, UK. Palaeontology 60, 349–374. https://doi.org/10.1111/pala.12288

Pálfy, J., Smith, P.L., 2000. Synchrony between Early Jurassic extinction, oceanic anoxic event, and the Karoo-Ferrar flood basalt volcanism. Geology 28, 747. https://doi.org/10.1130/0091-7613(2000)28<747:SBEJEO>2.0.CO;2

Poulton, S.W., 2021. The Iron Speciation Paleoredox Proxy, The Iron Speciation Paleoredox Proxy. Cambridge University Press. https://doi.org/10.1017/9781108847148

Poulton, S.W., Canfield, D.E., 2011. Ferruginous Conditions: A Dominant Feature of the Ocean through Earth's History. Elements 7, 107–112. https://doi.org/10.2113/gselements.7.2.107

Poulton, S.W., Canfield, D.E., 2005. Development of a sequential extraction procedure for iron: implications for iron partitioning in continentally derived particulates. Chem. Geol. 214, 209–221. https://doi.org/10.1016/j.chemgeo.2004.09.003

Richoz, S., van de Schootbrugge, B., Pross, J., Püttmann, W., Quan, T.M., Lindström, S., Heunisch, C., Fiebig, J., Maquil, R., Schouten, S., Hauzenberger, C.A., Wignall, P.B., 2012. Hydrogen sulphide poisoning of shallow seas following the end-Triassic extinction. Nat. Geosci. 5, 662–667. https://doi.org/10.1038/ngeo1539

Rudnick, R.L., Gao, S., 2014. Composition of the Continental Crust, in: Treatise on Geochemistry. Elsevier, pp. 1–51. https://doi.org/10.1016/B978-0-08-095975-7.00301-6

Ruhl, M., Bonis, N.R., Reichart, G.-J., Damsté, J.S.S., Kürschner, W.M., 2011. Atmospheric Carbon Injection Linked to End-Triassic Mass Extinction. Science. 333, 430–434. https://doi.org/10.1126/science.1204255

Ruhl, M., Deenen, M.H.L., Abels, H.A., Bonis, N.R., Krijgsman, W., Kürschner, W.M., 2010. Astronomical constraints on the duration of the early Jurassic Hettangian stage and recovery rates following the end-Triassic mass extinction (St Audrie's Bay/East Quantoxhead, UK). Earth Planet. Sci. Lett. 295, 262–276. https://doi.org/10.1016/j.epsl.2010.04.008

Simms, M.J., 2007. Uniquely extensive soft-sediment deformation in the Rhaetian of the UK: Evidence for earthquake or impact? Palaeogeogr. Palaeoclimatol. Palaeoecol. 244, 407–423. https://doi.org/10.1016/j.palaeo.2006.06.037

Simms, M.J., Jeram, A.J., 2007. Waterloo Bay, Larne, Northern Ireland: a candidate global stratotype section and point for the base of the Hettangian stage and Jurassic system. ISJS Newsl. 34, 50–68.

Swift, A., 1999. Stratigraphy (including biostratigraphy), in: Swift, A., Martill, D.J. (Eds.), Fossils of the Rhaetian Penarth Group. Field Guides to Fossils. Palaeontological Association, London, pp. 15–30.

Thibodeau, A.M., Ritterbush, K., Yager, J.A., West, A.J., Ibarra, Y., Bottjer, D.J., Berelson, W.M., Bergquist, B.A., Corsetti, F.A., 2016. Mercury anomalies and the timing of biotic recovery following the end-Triassic mass extinction. Nat. Commun. 7, 11147. https://doi.org/10.1038/ncomms11147

Tribovillard, N., Algeo, T.J., Baudin, F., Riboulleau, A., 2012. Analysis of marine environmental conditions based onmolybdenum–uranium covariation—Applications to Mesozoic paleoceanography. Chem. Geol. 324–325, 46–58. https://doi.org/10.1016/j.chemgeo.2011.09.009

Ward, P.D., Garrison, G.H., Haggart, J.W., Kring, D.A., Beattie, M.J., 2004. Isotopic evidence bearing on Late Triassic extinction events, Queen Charlotte Islands, British Columbia, and implications for the duration and cause of the Triassic/Jurassic mass extinction. Earth Planet. Sci. Lett. 224, 589–600. https://doi.org/10.1016/j.epsl.2004.04.034

Wignall, P.B., 2015. The Worst of Times: How Life on Earth Survived Eighty Million Years of Extinctions. Princeton University Press, Princeton and Oxford.

Wignall, P.B., Atkinson, J.W., 2020. A two-phase end-Triassic mass extinction. Earth-Science Rev. 208, 103282. https://doi.org/10.1016/j.earscirev.2020.103282

Wignall, P.B., Bond, D.P.G., 2008. The end-Triassic and Early Jurassic mass extinction records in the British Isles. Proc. Geol. Assoc. 119, 73–84. https://doi.org/10.1016/S0016-7878(08)80259-3

Wignall, P.B., Bond, D.P.G., Kuwahara, K., Kakuwa, Y., Newton, R.J., Poulton, S.W., 2010. An 80 million year oceanic redox history from Permian to Jurassic pelagic sediments of the Mino-Tamba terrane, SW Japan, and the origin of four mass extinctions. Glob. Planet. Change 71, 109–123. https://doi.org/10.1016/j.gloplacha.2010.01.022